Astrophysics and Space Science (2023) 368:20
https://doi.org/10.1007/s10509-023-04170-w

RESEARCH

A standalone prediction model for atomic oxygen and coronal mass ejections

W.M. Mahmoud[1] · D. Elfiky[2] · S.M. Robaa[3] · M.S. Elnawawy[3] · S.M. Yousef[3]

Received: 7 August 2022 / Accepted: 3 March 2023 / Published online: 22 March 2023

Abstract
This paper presents a standalone predictive model for Atomic Oxygen (AO), Coronal Mass Ejections (CMEs) and other space-environment parameters. The prediction is based on the numerical method of Holt–Winter's triple smooth exponential forecasting of atmospheric constituents. Solar cycle 25 is likely to show about the same activity as cycle 23. The corresponding AO-flux–solar-activity correlation coefficients for altitudes 100, 200, and 300 km are: 0.62, 0.53, and 0.48, respectively, while the correlation coefficients for higher altitudes are lower than 0.48, an advantage that makes them more favorable for LEOs due to the harmful corrosive effects.

Keywords Atomic Oxygen (AO) · Standalone prediction model · Low-Earth Orbits · Coronal Mass Ejections

1 Introduction

Satellite protection depends greatly on accurate predictions of the surrounding space-environment components and hazards. The space environment of the Low-Earth Orbits (LEOs) is highly affected by solar activity. Solar activity is the key factor affecting the space environment. Assessment of the space environment depends strictly on three subprocesses or consecutive steps. The first step is the study of all components of the environment of the space mission by addressing all questions about that mission (orbit, start time, duration, solar activity, type of mission, etc.). Secondly, detailed investigations of all the mission components should be done. The final step it to use all the analysis done to protect the mission in order to fulfill its target. Satellite protection requires full prediction of all the constraints and worst-case scenarios related to the mission. The prediction may be developed using deep learning, machine learning or statistical analyses.

During solar-activity cycles particle, radiation, and magnetic fluxes in the heliosphere change, which cause different space-weather effects at Earth. Prediction of the solar-activity cycle is therefore the main step in protecting space missions and satellite technology (Bhowmik and Nandy 2018). Space weather influences the electromagnetic environment around Earth and human life. Many space-weather events that are caused by solar eruptions, are potential risks to the social infrastructure such as aviation, communications, artificial satellites, electric power, and positioning systems (Kusano et al. 2021). Solar cycles 23 and 24 were weak cycles at the bottom of the 80–120 years long-term Wolf–Gleissberg solar cycle (Yousef 2006), (Mawad 2017), (Yousef et al. 2018), and (Mawad and Abdel-Sattar 2019).

1.1 Atomic Oxygen (AO)

Previously, it was shown through various studies that solar activity has a strong influence on the ionosphere (Mawad

✉ D. Elfiky
delfiky@narss.sci.eg

W.M. Mahmoud
wael.mohamed@egsa.gov.eg

S.M. Robaa
robaa@sci.cu.edu.eg

M.S. Elnawawy
msnawawy@sci.cu.edu.eg

S.M. Yousef
Shahinazmostafa15@yahoo.com

1 Assembly, Integration and Testing, AIT Center at Egyptian Space Agency, EgSA, Cairo, Egypt

2 Thermal, structure and space environment dep. at National Authority of Remote Sensing and Space Sciences, NARSS, Cairo, Egypt

3 Meteorology, Astronomy and Space department faculty of Science Cairo University, Giza, Egypt

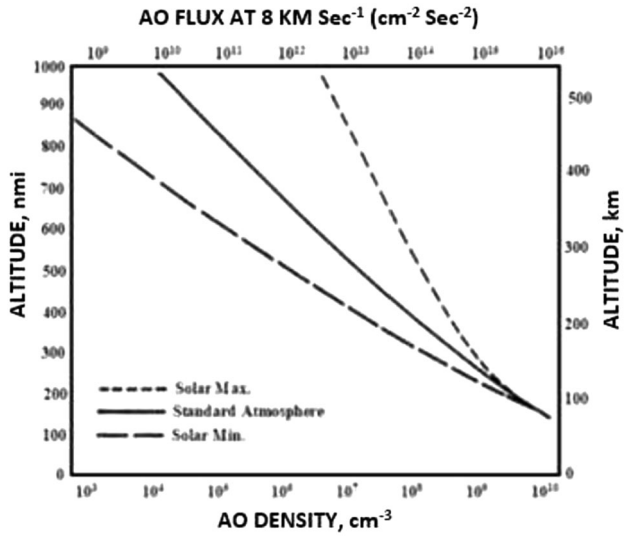

Fig. 1 Relation between AO and solar activity [11]

2015) and (Farid et al. 2020). Solar activity has the greatest impact on AO density in the ionospheric layers leading to the enhancement of the erosion depths for material surfaces directly exposed to AO. The density and flux values of AO are higher during maximum solar activity than at minimum. The average fluence of AO per year and the corresponding erosion depth varies in response to solar-activity variations within the solar cycle (Samwell 2014) and (Farid et al. 2015) as shown in Fig. 1. In general, AO, hence O+, are the dominant species in the LEO environment. It is anticipated that as solar-flare events reach Earth, they enhance O and O+. Oxygen atoms have high corrosive power during and after combining with the material. According to the satellite's orbital velocity of 7.8 km/s in LEO, the satellite is exposed to very strong streams of AO at energies in the range of 5 eV (Dooling and Finckenor 1999) and (Mahmoud et al. 2021).

1.2 Coronal Mass Ejections

Coronal Mass Ejections (CMEs) are powerful eruptions of magnetic flux and plasma from the Sun into interplanetary space (Liu et al. 2020). The most powerful CMEs and their associated flares have very strong impacts on the near-Earth environment, affecting the lifetime of space technology, (Baker et al. 2004) and (Mawad et al. 2014). Many efforts should be made to develop new models for forecasting CMEs, (Bobra and Ilonidis 2016) and (Inceoglu et al. 2018).

Predicting the lifetime of the LEO satellites is of great concern to the satellite industry and technology. All LEO satellites suffer orbital decay due to their interactions with the Earth's atmosphere. The single-exponential smoothing method and the single moving-average method were applied to the sample as used in Aknil (Hudaningsih et al. 2020) and (Khodairy et al. 2020). The two methods were used to compare the most accurate forecasting methods close to their actual values. Previous studies used empirical methods for prediction of the travel time of interplanetary Coronal Mass Ejection Shocks (ICME) such as (Youssef et al. 2011). Also, many studies used the empirical methods to investigate the CME occurrence in accordance with the solar flare. Other studies used artificial-intelligence networks to detect the arrival time of interplanetary coronal mass ejection shocks during solar cycles, (Mawad et al. 2016). For this study, to present numerical predictions for CMEs characteristics empirical methods were used.

The main objective of this study is to develop a standalone predictive model for the space-environment parameters and compare the results with real data.

2 Methodology and data sources

Statistical analyses and forecasting techniques depend on gathering historical data and finding the pattern (trend or seasonal variation) and determining the forecasting method. Following forecasting calculations, a verification step is required to assure the accuracy and precision of the prediction model.

The Holt–Winters method is used by many companies to produce short-term forecasts as their sales data contain a trend or seasonal pattern. This method is simple, easily automated, and has low data-storage requirements. The Holt–Winters method was applied to the air-transportation industry. The time series was decomposed into three additive components: trend, seasonal, and remainder. Multiple regression may be recognized as a better forecasting method for daily and weekly short-term forecasting, whereas Holt–Winters methods presented better forecasting values for monthly and yearly long-term forecasting (Tratar and Strmčnik 2016). Due to strong seasonal variation detected in the series, the Holt–Winters method can be used (Dantas et al. 2017).

Our data source is obtained from the Naval Research Laboratory for Mass Spectrometer and Incoherent Scatter Radar (NRLMSISE-00) Atmosphere Model (5) during the period 1996 to 2020 for the atmosphere. The data includes sunspot number, density, temperature, and flux of H-atoms cm^{-3}, He-atoms cm^{-3}, N-atoms cm^{-3}, oxygen atoms cm^{-3}, AO atoms cm^{-3}, atomic N-atoms cm^{-3}, and Ar-atoms cm^{-3}. The altitude resolution is 50 km and the date step size is 7 days, i.e., three observations per month. The data under study covers the period of solar cycles 23 and 24.

Segregation of data by altitude levels is then done by skipping altitudes under 100 km out of the LEO region. The

observations are also taken at latitude 0.0° from the Earth's surface and from 0 km to 1000 km above the Earth's surface. The specified location [equator] at the Earth's surface is due to the geoid shape of the Earth's atmosphere. In other words, the greater the atmospheric altitude, the more space hazards occur. The equator has the highest locations in the atmosphere. The data time series was plotted.

Data regression is required. Without equations governing the variation of atmospheric properties and interpolation with time, the best way is to apply numerical analyses methods to drive the regression for such properties. The building and developing of the model depend on about 60% of the data, while the remainder 40% are used in its verification.

Careful analyses of the data are required. The data are plotted in Fig. 2, showing seasonal variations. It shows the correlation relation between the solar activity and AO flux for altitudes 100 km, 500 km, and 1000 km. The relations between sunspot number (SSN) and the property of the atmosphere reveals that the variation is the solar cycle. The visual inspection of graphs indicates the strong relation between AO density and the solar activity for altitudes 500 km and 1000 km, while for 100 km, the relation became more stable during the solar cycle except for minimum solar activity. In other words, the AO flux is more favorable for lower altitudes, The solar cycle is mainly about 11 years [about 132 months], i.e., every 132 rows, there is a new cycle. Thus, the regression method must be a seasonal method. There is a variety of seasonal regression methods such as Holt–Winter's seasonal additive method, Holt–Winter's seasonal multiplication method, exponential regression, and the Triple-Exponential Smoothing method.

On trying most of these methods, the chosen one is the Triple-Exponential Smoothing method, depending on the lowest error value. The basic equations of this method are:

$$S_t = \frac{y_t}{I_{t-L}} + (1-\alpha)\,(S_{t-1} + b_{t-1}) \quad \text{Overall Smoothing} \tag{1}$$

$$b_t = \gamma\,(S_t - S_{t-1}) + (1-\gamma)\,b_{t-1} \quad \text{Trend Smoothing} \tag{2}$$

$$I_t = \beta\frac{y_t}{S_t} + (1-\beta)\,I_{t-L} \quad \text{Seasonal Smoothing} \tag{3}$$

$$F_{t+m} = (S_t + mb_t)\,I_{t-L+m} \quad \text{Forecast.} \tag{4}$$

We define:
– y is the observation
– S is the smoothed observation
– b is the trend factor
– I is the seasonal index
– F is the forecast at m periods ahead
– t is an index denoting a time period

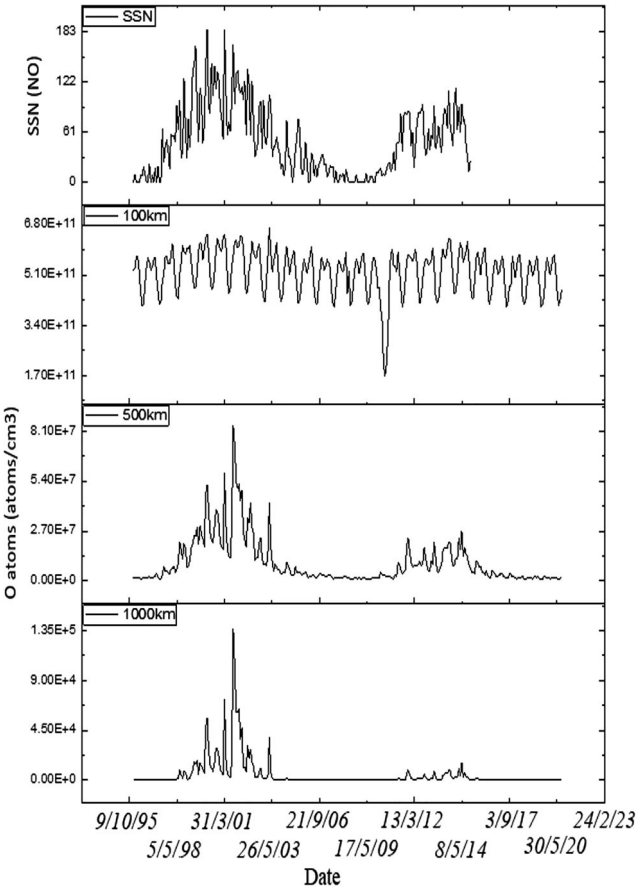

Fig. 2 AO levels comparison with SSN from (9/10/95) to (30/5/20) for altitudes of 100, 500, and 1000 km above Earth's surface

and α, γ, and β are constants that must be estimated in such a way that the mean squared error (MSE) of the error is minimized.

Based on equations (1), (2), (3), and (4), the forecasting of solar-activity cycle 25 is extracted as shown in Figs. 3 and 4. Figures 3 and 4 present a description for the prediction method in the software.

It is evident from both Fig. 3 and Fig. 4 that cycle 25 is likely to be almost as active as cycle 23.

The prediction model for atmospheric density, temperature, and AO fluxes is based on differential equations as follows:

Atmospheric Pressure (P)

$$P = \frac{F}{A} = \rho g h \tag{5}$$

$$\frac{d\rho}{\rho} = -\frac{g}{RT}dh \tag{6}$$

$$\rho = \rho_0 e^{(-\frac{h}{H})}, \tag{7}$$

where, ρ is the density, g is the gravitational constant, h is the altitude in the atmosphere, F is the net force, A is the

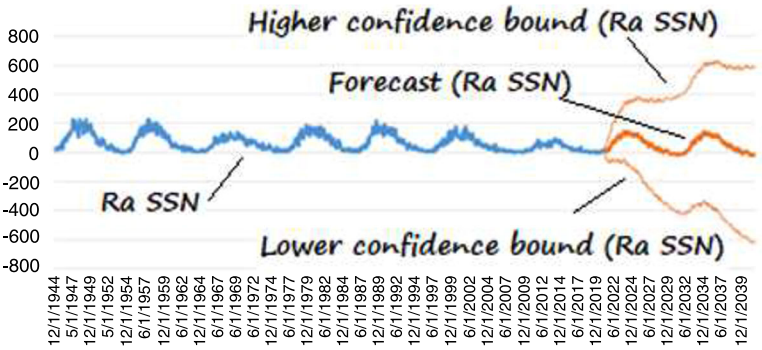

Fig. 3 Forecast of lower and higher confidence bound for solar cycle 25

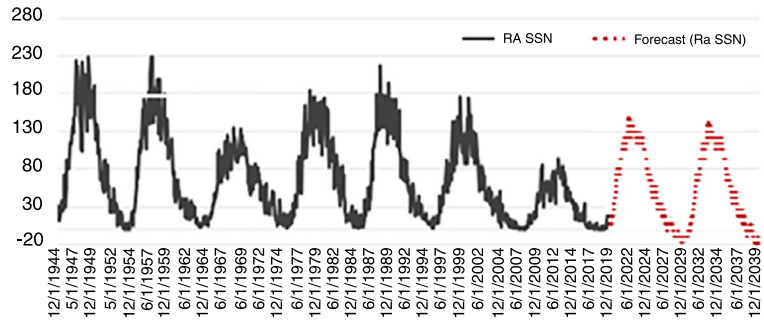

Fig. 4 Extraction for the forecasting of solar-activity cycle 25

cross-sectional area, R is the universal gas constant, and T is the temperature

Atmospheric Temperature (T)

$$\overline{v}_a = \sqrt{\frac{8k_bT}{\pi\overline{M}}}, \qquad v_{rms} = \sqrt{\frac{2k_bT}{\overline{M}}}, \quad v_P = \sqrt{\frac{2k_bT}{\overline{M}}} \tag{8}$$

$$\frac{4}{\pi}k_bT = \frac{1}{2}\overline{M}\overline{v}_a^2, \qquad \frac{3}{2}k_bT = \frac{1}{2}\overline{M}v_{rms}^2,$$

$$k_bT = \frac{1}{2}\overline{M}v_P^2, \tag{9}$$

where, $\overline{v}_a$ is the average thermal speed, v_{rms} is the root-mean-square speed, and v_p is the most probable speed of an air molecule ($\mathrm{m\,s^{-1}}$). These speeds are related to absolute temperature.

Atomic Oxygen

$$\rho = 4.39 \times 10^{-16}x + 2.91 \times 10^{-14},$$

$$\mathrm{AO} = 3.39 \times 10^{8}x^{0.342}, \quad \text{and}$$

$$T = 681 + 3.36x - 6.82 \times 10^{-3}x^2 \tag{10}$$

for density, atomic oxygen, and temperature, respectively, where x is the SSN number.

$$\rho = 6.33 \times 10^{-18}x^{0.968}, \quad \mathrm{AO} = 175281x^{1.02}, \quad \text{and}$$

$$T = 686 + 3.53x - 6.57 \times 10^{-03}x^2 \tag{11}$$

for density, atomic oxygen, and temperature, respectively at 500 km.

$$\rho = 9.16 \times 10^{-19} + 9.6810^{-21}x + 8.63 \times 10^{-23}x^2,$$

$$\mathrm{AO} = 0.213x^{2.26}, \quad \text{and}$$

$$T = 686 + 3.53x - 6.58 \times 10^{-03}x^2 \tag{12}$$

for density, atomic oxygen, and temperature, respectively, at 1000 km, where x is the SSN number and ρ is the AO density

Root Mean Square (RMS)

$$\mathrm{RMS} = \sqrt{\frac{1}{n}\sum_{i=1}^{n}(R_i - P_i)^2}. \tag{13}$$

3 Results and discussion

In order to initialize the Triple-Exponential Smoothing method, we need at least one complete set of a solar cycle's data to determine initial estimates of the solar cycle's indices I_{t-L}.

All the above-discussed methods have been used for forecasting atmospheric constituents (He, Ar, O molecules, AO, N molecules, N atoms, and/or H), solar irradiance, orbital lifetime (semimajor axis, eccentricity and/or density drag), coronal mass ejections (linear speed, central PA, mass

Table 1 The RMS and the correlation coefficient for ρ, T, and H-atoms from (01/10/2020) to (01/06/2021)

Altitude (km)	RMS			Correlation coefficients		
	ρ	T	H atoms	ρ	T	H atoms
1000	5.65E-20	17.73	3394.56	0.73	0.03	0.18
950	2.39E-19	17.73	3961.92	0.62	0.03	0.20
900	3.32E-19	17.73	4619.04	0.63	0.03	0.22
850	4.93E-19	17.73	5354.80	0.66	0.03	0.23
800	7.9E-19	17.73	6153.57	0.67	0.03	0.25
750	1.4E-18	17.73	7073.07	0.62	0.03	0.27
700	2.14E-18	17.73	8112.84	0.76	0.03	0.28
650	3.72E-18	17.73	9253.69	0.66	0.03	0.29
600	7.4E-18	17.73	10575.08	0.55	0.03	0.31
550	1.98E-17	17.73	12055.62	0.36	0.03	0.32
500	4.28E-17	17.73	13680.28	0.32	0.03	0.33
450	7.59E-17	17.73	15530.98	0.43	0.03	0.34
400	2.23E-16	17.71	17590.89	0.35	0.03	0.35
350	5.45E-16	17.66	19943.83	0.41	0.03	0.36
300	1.42E-15	17.57	22594.08	0.49	0.03	0.37
250	3.71E-15	16.49	25790.77	0.60	0.22	0.38
200	1.22E-14	16.13	32067.74	0.66	0.11	0.40
150	1.97E-14	13.56	74115.16	0.62	0.21	0.55
100	1.76E-11	3.51	544961.24	0.82	0.71	0.86

and/or angular width), debris hazards, the orbital visualization as well as density and temperature, T.

The results of the software (S/W) are verified by comparison of the predicted data from S/W with the real data from NRLMSISE-00. The last date in the database of the S/W is 01/09/2020 and the verification was done on 01/06/2021. RMS and the correlation coefficients are calculated for ρ, T, and H-atoms as shown in Table 1.

Table 2 displays the crosscorrelation between real and forecasted data for CMEs' position central angle PA (deg), angular width (deg), linear speed (km/s), and measurement position angle MPA (deg). PA is the four categories of position angle 90°, 180°, 270°, and 360°.The optimum correlation and an optimum number of lags are shaded. The lag is equal 7 days. Detailed comparisons for CMEs' central PA (deg), angular width (deg), linear speed (km/s), and MPA (deg) are displayed in Figs. 5, 6, 7, and 8, respectively.

For AO forecasting and comparison with real data, see Table 3 and Figs. 9, 10, and 11 for altitudes 100, 200, and 300 km, respectively. The rest of the altitudes (from 350 km to 1000 km) do not give a strong correlation.

The high correlation-coefficient values for lower altitudes indicates the presence of atomic oxygen in abundance at such altitudes, in contrast to its presence in limited quantities at higher altitudes.

Table 2 Crosscorrelation between real and forecasted data for CMEs from (02/09/2020) to (30/11/2021)

Lag	Central PA	Width	Linear speed	MPA
0	0.02673272	−0.03143	0.084329623	0.008715
1	0.09253402	0.119283	0.219283	0.093747
2	0.20943581	0.328394	0.398372	0.293046
3	0.49231581	0.529283	0.7018273	0.397452
4	0.68490214	0.059283	0.1928347	0.529485
~~5~~	0.19820175	−0.19384	−0.29384	−0.23848
6	−0.2039485	−0.08393	−0.092374	−0.03488

Table 3 Comparison of AO real and forecasted fluxes from 01/01/2021 to 01/12/2021

Altitude (km)	Correlation coefficient
100	0.62
200	0.53
300	0.48

4 Conclusion

Solar cycle number 25 is likely to have about the same activity as cycle 23. However, unexpected strengthening of solar cycle 25 is not excluded. If that is the case, then the applied predictive models should be modified accordingly to fit the observations.

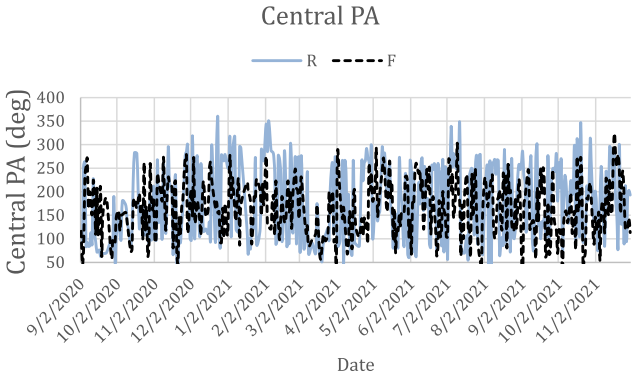

Fig. 5 Measured and forecasted data for the CMEs central PA (deg) from (02/09/2020) to (30/11/2021)

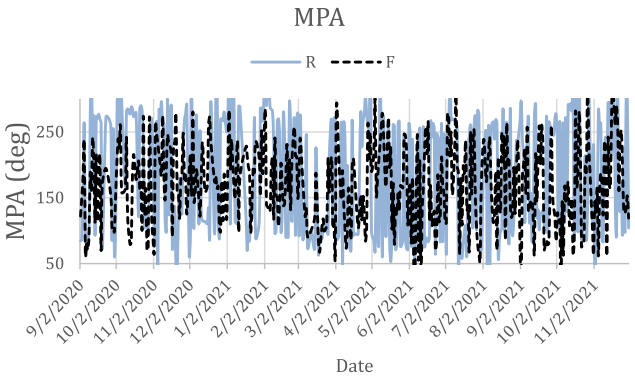

Fig. 8 Measured and forecasted data for the CMEs MPA (deg) from (02/09/2020) to (30/11/2021)

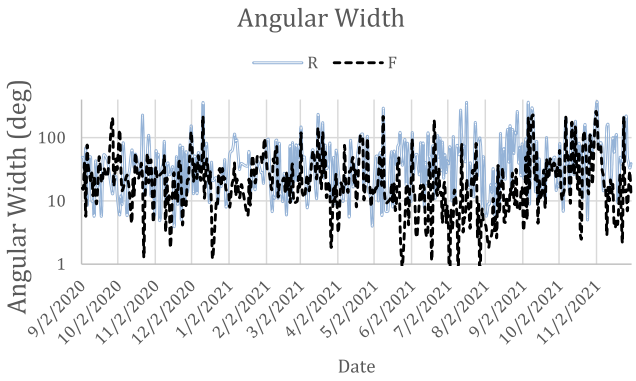

Fig. 6 Measured and forecasted data for the CMEs angular width (deg) from (02/09/2020) to (30/11/2021)

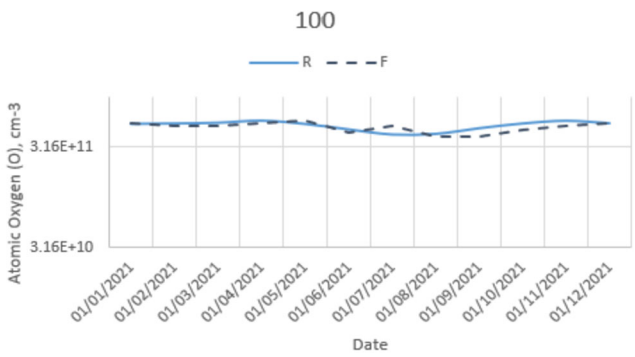

Fig. 9 Measured and forecasted data for the AO fluxes for 100 km altitude from (02/09/2020) to (30/11/2021)

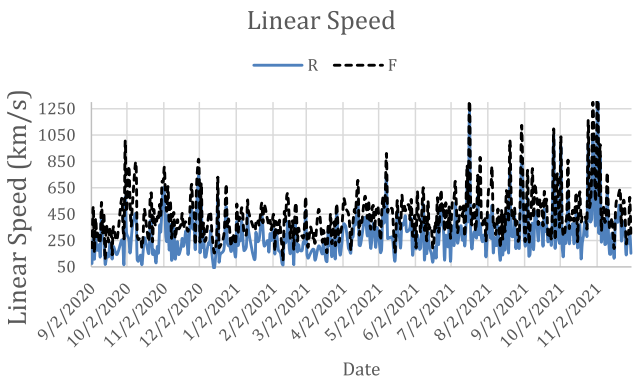

Fig. 7 Measured and forecasted data for the CMEs linear speed (km/s) from (02/09/2020) to (30/11/2021)

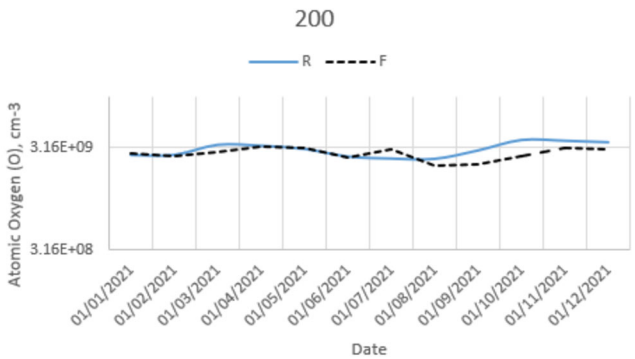

Fig. 10 Measured and forecasted data for the AO fluxes for 200 km altitude from (02/09/2020) to (30/11/2021)

By applying the crosscorrelation for CMEs, with a lag of 7 days, the Central PA shows a value of 0.68 with lag number 4. The Angular width shows a value of 0.53 with the lag number 3. The linear speed shows a value of 0.7 with the lag number 3. The MPA shows a value of 0.53 with the lag number 4.

AO is the most abundant species for the near LEOs. The corresponding AO-flux–solar-activity correlation coefficients for altitudes 100, 200, and 300 km are: 0.62, 0.53, and 0.48, respectively.

The altitudes from 350 km to 1000 km do not give a strong correlation for the AO fluxes forecasting, an advantage that makes them more favorable for LEOs due to the harmful corrosive effects.

The model of AO forecasting needs more modifications and refinements by adding more parameters and other trending and seasonal variations.

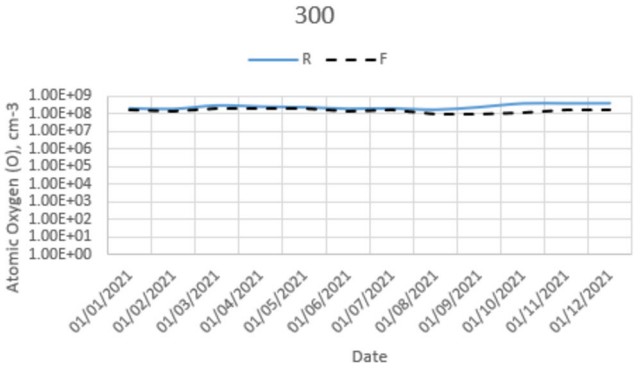

Fig. 11 Measured and forecasted data for the AO fluxes for 300 km altitude from (02/09/2020) to (30/11/2021)

Recommendation

This research recommends continuous development and improvement of predictive models for solar activity and space-environment components. In addition, many S/W verifications are required.

Acknowledgement The authors would like to express their deep and sincere gratitude to Islam Reda Ahmed, Mahmoud Adel Mohamed, Mustafa Saied El_Sayed, and Rahma Ashraf Khalil. Their dynamism, vision, sincerity, and motivation have deeply inspired us.

Author contributions W.M. Mahmoud wrote the main manuscript text. Dalia Elfiky prepared data and figures. All authors reviewed the manuscript.

Funding Note Open access funding provided by The Science, Technology & Innovation Funding Authority (STDF) in cooperation with The Egyptian Knowledge Bank (EKB).

Declarations

Competing interests The authors declare no competing interests.

References

Baker, D., Daly, E., Daglis, I., Kappenman, J., Panasyuk, M.: SpWea **2**, S02004 (2004).

Bhowmik, P., Nandy, D.: Prediction of the strength and timing of sunspot cycle 25 reveal decadal-scale space environmental conditions. Nat. Commun. **9**, 5209 (2018). https://doi.org/10.1038/s41467-018-07690-0

Bobra, M., Ilonidis, S.: Astrophys. J. **821**, 127 (2016)

Dantas, T., Oliveira, F., Repolho, H.: Ar transportation demand forecast through Bagging Holt Winters methods. J. Air Transp. Manag. **59**, 116–123 (2017). ISSN 0969 6997. https://doi.org/10.1016/j.jairtraman.2016.12.006.

Dooling, D., Finckenor, M.: Material selection guide lines to limit atomic oxygen effects on spacecraft surfaces (1999). NASA/TP-1999-209260, NASA Technical Publication

Farid, H., Mawad, R., Ghamry, E., Yoshikawa, A.: The impact of coronal mass ejections on the seasonal variation of the ionospheric critical frequency f0F2, universe 2020. Special Issue for Space Weather **6**(11), 200 (2020). https://doi.org/10.3390/universe6110200

Farid, H., Mawad, R., Yousef, M., Yousef, S.: The impacts of CMEs on the ionospheric critical frequency foF2. Elixir Space Sci. **80**, 31067–31070 (2015). http://adsabs.harvard.edu/abs/2015ElSS...8031067F

Hudaningsih, N., Utami, F., Abdul Jabbar, W.: Perbandingan peramalan penjualan produk Aknil Pt. sunthi sepurimengguanakan metode single moving average dan single exponential smooting. JINTEKS **2**(1), 15–22 (2020)

Inceoglu, F., Jeppesen, J., Kongstad, P., Hernández, M., Jacobsen, R., Karoff, C.: Using machine learning methods to forecast if solar flares will be associated with CMEs and SEPs. Astrophys. J. **861**, 128 (2018)

Khodairy, S., Sharaf, M., Awad, M., Abdel Hamed, R., Hussein, M.: J. Phys. Conf. Ser. **1523**, 012010 (2020)

Kusano, K., Ishii, M., Berger, T., Miyoshi, Y., Yoden, S., Liu, H., Onsager, T., Ichimoto, K.: Special issue "Solar–terrestrial environment prediction: toward the synergy of science and forecasting operation of space weather and space climate". Earth Planets Space **73**, 198 (2021). https://doi.org/10.1186/s40623-021-01530-0

Liu, H., Liu, C., Wang, J., Wang, H.: Predicting coronal mass ejections using SDO/HMI vector magnetic data products and recurrent neural networks. Astrophys. J. **890**, 12 (2020). 9pp

Mahmoud, W., Elfiky, D., Robaa, S., Elnawawy, M., Yousef, S.: Effect of atomic oxygen on Leo CubeSat. Int. J. Aeronaut. Space Sci. **22**, 726–733 (2021)

Mawad, R., Abdel-Sattar, W.: The eruptive latitude of the solar flares during the Carrington rotations (CR1986-CR2195). Astrophys. Space Sci. **364**, 197 (2019). https://doi.org/10.1007/s10509-019-3683-0

Mawad, R.: On the correlation between Earth's orbital perturbations and oscillations of sea level and concentration of greenhouse gases. J. Mod. Trends Phys. R. **15**(MTPR-14), 1–9 (2015). https://doi.org/10.19138/mtpr/(15)1-9. http://adsabs.harvard.edu/abs/2015JMTPR..15....1M

Mawad, R.: Coherence between sea level oscillations and orbital perturbations. Earth Space Sci. **4**(3), 138–146 (2017). https://doi.org/10.1002/2016EA000198. http://adsabs.harvard.edu/abs/2017E&SS....4.138M

Mawad, R., Farid, H., Yousef, S.: The Impacts of Halo-CMEs on the Ionospheric Critical Frequency foF2, APS April Meeting 2016, abstract id. L1.012 (2014) ADS: 2016APS..APR.L1012M

Mawad, R., Radi, A., Mahrous, A., Youssef, M.: Detection of interplanetary coronal mass ejections' signature using artificial neural networks. J. Mod. Trends Phys. R. **16**, 1–10 (2016). https://doi.org/10.19138/mtpr/(16)1-10

Samwell, S.: Low Earth Orbital Atomic Oxygen Erosion Effect on Spacecraft (2014)

Tratar, L.F., Strmčnik, E.: The comparison of Holt–Winters method and multiple regression method: a case study. Energy **109**, 266–276 (2016). https://doi.org/10.1016/j.energy.2016.04.115

Yousef, S.: 80 120 yr long-term solar induced effects on the Earth, past and predictions. Phys. Chem. Earth **31**(1–3), 113–122 (2006)

Yousef, S., Mawad, R., Robaa, S., Teama, D., Moheb El-Dine, M., Saber, R., Elfaki, H.: Right now, we are on the brink of an ice age in Europe and America and a rainy epoch on the Sahara and Arabia. In: AGU 2018 Fall Meeting, Washington, Monday, 10 December 2018; abstract 468811, C13I-1250, Session C13I-1250: Quantifying Spatial and Temporal Variability of Snow and Snow Processes (2018). https://doi.org/10.13140/RG.2.2.28879.74407.

Youssef, M., Shaltout, M., Mawad, R.: Empirical model of the travel time of interplanetary coronal mass ejection shocks. NRIAG J. Astron. Astrophys., Special Issue **5**, 47–61 (2011). https://doi.org/10.1007/s42405-020-00336-w. Materials. Space Res. J. **7**(1), 1–13